A NEW FACILITY FOR STUDYING SHOCK WAVE PASSAGE OVER DUST LAYERS

A Thesis

by

BRANDON DAVID MARKS

Submitted to the Office of Graduate Studies of
Texas A&M University
in partial fulfillment of the requirements for the degree of

MASTER OF SCIENCE

Chair of Committee,	Eric L. Petersen
Co-Chair of Commitee,	M. Sam Mannan
Committee Member,	Devesh Ranjan
Head of Department,	Andreas A. Polycarpou

August 2013

Major Subject: Mechanical Engineering

ABSTRACT

To ensure safety regarding dust explosion hazards, it is important to study the dust lifting process experimentally and identify important parameters that will be valuable for development and validation of numerical predictions of this phenomenon. A new shock tube test section was developed and integrated into an existing shock tube facility. The test section allows for shadowgraph or laser scattering techniques to track dust layer particle motion. The test section is designed to handle an initial pressure of 1 atm with an incident shock wave velocity up to Mach 2 to mimic real world conditions. The test section features an easily removable dust pan and inserts to allow for adjustment of dust layer thickness. The design allows for the changing of experimental variables including initial pressure, Mach number, dust layer thickness and characteristics of the dust itself. A separate vacuum manifold was designed to protect existing equipment from negative side effects of the dust. A study was performed to demonstrate the capabilities of the new facility and to compare results with experimental trends formerly established in the literature. Fourty-micron limestone dust with a layer thickness of 3.2 mm was subjected to Mach 1.22 and 1.38 shock waves, and a high-speed shadowgraph was used for flow visualization. Dust layer rise height was graphed with respect to shock wave propagation. Dust particles subjected to a Mach 1.38 shock wave rose more rapidly and to a greater height with respect to shock wave propagation than particles subjected to a Mach 1.22 shock wave. These results are in agreement with trends found in the literature, and a new area of investigation was identified.

ACKNOWLEDGEMENTS

I would like to thank my adviser and committee chair, Dr. Petersen for his guidance, feedback and faith in my abilities. I would also like to thank my other committee members, co-chair Dr. Mannan and member Dr. Ranjan.

Thanks also to my co-workers, Amira Chowdhury for her assistance, and Sankar Ravi, Anibal Morones, and Kenny McCown for their help in installing the equipment. I would like to thank Olivier Mathieu for his help with studies unrelated to this work. I also want to extend my gratitude to the Mark Kay O'Connor Process Safety Center at Texas A&M for providing funding and making this project possible. Also, I thank the rest of my colleagues and professors for making Texas A&M a great experience.

Last but not least I would like to thank my cousins and family in Austin for providing a home away from home, my mother for her encouragement, and my girlfriend for her love, patience and wisdom.

NOMENCLATURE

a_1	Speed of sound through gas in zone 1
a_2	Speed of sound through gas in zone 2
k	1.4, specific heat ratio of air
M_2	Mach number of flow in zone 2
M_i	Mach number of incident shock wave
M_r	Mach number of reflected shock wave
P_1	Pressure of shock tube zone 1
P_2	Pressure of shock tube zone 2
P_5	Pressure of shock tube zone 5
R	287 (N-m)/(kg-K), Ideal gas constant
T_1	Temperature of shock tube zone 1
T_2	Temperature of shock tube zone 2
T_5	Temperature of shock tube zone 5
t_{obs}	Maximum experiment observation duration
V_i	Velocity of incident shock wave
V_r	Velocity of reflected shock wave
X_0	Location of observation reference location
X_c	Location where reflected shock and fluid contact surface cross
X_e	Shock tube driven section length
X_s	Location of incident shock wave

Y_d	Dust particle height; height of dust layer boundary

TABLE OF CONTENTS

LIST OF FIGURES

Page

LIST OF TABLES

Page

1. INTRODUCTION

1.1 Motivation

Dust explosions are a real danger in process industries. Coal dust explosions present a significant safety hazard to the coal mining industry. Grain dust explosions are a hazard in agricultural industries, and metal dust can also present a dust explosion hazard. Factors influencing dust explosibility include particle size, dust concentration, oxidant concentration, ignition temperature, turbulence, rate of pressure rise, admixed inert dust, and the presence of flammable gasses. There are many possible dust explosion triggers such as flames and direct heat; self-heating; hot work; incandescent material; hot surfaces; electro static and electrical sparks; friction and hot sparks; impact sparks; static electricity, lightning and shock waves (Abbasi & Abbasi, 2007). Often, dust explosions are secondary explosions triggered by some other initial event. A primary event may lead the agitation of dust particles and lift them into the air. Air is often the primary oxidizer in these reactions, and the mixture of fine dust particles and air may be highly combustible. At the onset of combustion, a pressure wave may precede the flame front, initiating the mixing of dust and air ahead of the flame resulting in self-propagation of the phenomenon. Understanding the mechanisms that govern dust layer and fluid stream interactions is important to limit the risks of dust explosions within process industries. To further the understanding of dust layer fluid interactions, a new experimental facility has been developed.

1.2 Experimental Studies

Former experimental works have studied the interaction of unsteady dust layers with gas flows (shock waves, compression and expansion waves). Much attention has been given to understanding the phenomenon of dust lifting. Gerrard concluded that dust entrainment is the result of shock wave passage through the dusty layer (Gerrard, 1963). Fletcher investigated the claims of Gerrard and concluded through experimentats and theoretical analysis that the primary mechanism of dust lifting is the rapid flow behind the propagating shock across the surface of the dust, instead of shock wave propagation through the dust layer as suggested by Gerrard (Fletcher, 1963). Bracht and Merzkirch identified the governing force in dust lifting is the Saffman force and supported their experimental work with a numerical model (Merzkirch & Bracht, 1978). Bracht attempted to predict the development of dust mass concentrations in unsteady air flow and concluded that the predictions "depend on a number of data which can be determined only by means of experiments" (Bracht & Merzkirch, 1979). Hwang studied the interaction of a coal-dust layer with a weak shock wave passing above it using high speed photography (Hwang, 1982). The effect of particle size on dust dispersion and Magnus force has also been investigated (Suzuki & Adachi, 1984) (Boiko & Papyrin, 1987). Fedorov in his review paper discussed a variety of works related to shock interaction with dust layers and concluded that the dust lifting from a packed bed does not depend on the layer depth, but that curving of the layer surface and particle density have important effects on the lifting of dust particles (Fedorov, 2004).

Other studies have focused on the dust lifting problem connected with combustion problems and detonation, usually called a 'layered' detonation. In 2005, Klemens et al. studied shock interactions with coal dust and silica dust in a shock tube to identify important parameters such as the time delay in lifting the dust from the layer and dust concentration behind the propagating shock (Klemens, et al., 2006).

1.3 Numerical Studies

The process of dust lifting and two phase flows were also comprehensively studied numerically. However, there is no mathematical model that could describe all stages of the process of dust lifting, including propagation of wave processes in the layer retaining cohesion, processes of turbulent mixing, and specific features of force interaction of the phases (Fedorov, 2004). A direct numerical simulation of the turbulent boundary layer formation was performed by Kuhl et al. and found that the dense gas approximation is an accurate model of two phase dusty layer flows (Kuhl, et al., 1990). Fedorov developed a model of an equilibrium heterogeneous medium with allowances for turbulence and verified the model by comparisons with experimental dependencies of pressure on the substrate (Fedorov & Fedorchenko, 2005). GexCon released the first version of the CFD code, DESC 1.0, in June 2006 which has been used to develop a dispersion model of coal dust behind a propagating shock wave (Skjold, 2007). Fan conducted a numerical study in conjunction with an experimental study and concluded that the dense, two-phase flow model developed by Gidaspow from the kinetic theory, has proven to be valid for the description of the interaction of a shockwave with a dusty mass layer (Gidaspow,

1994) (Fan, et al., 2007). Ilea et al. incorporated polydispersity effects by modeling dust lifting behind a propagating shock wave using an Eulerian–Lagrangian method (Ilea, et al., 2009). Much effort has been given towards numerical analysis of the dust dispersion phenomenon, and as new methods and models are developed, experimental validation is required.

1.4 Thesis Outline

The next section of the thesis will cover the facility design, giving an overview of shock tube physics, special considerations specific to dusty gas experiments followed by design specifications. Following will be an outline of the experimental setup including experimental variables, the optical arrangement, shockwave characterization and details the procedure used in this study. A results and discussion section with suggested recommendations precede the ending summary. The thesis ends with the references and appendix sections.

2. FACILITY DESIGN

2.1 Shock Tube Physics

The shock tube facility used in this work is a diaphragm-driven shock tube. The Shock tube is composed of two co-linear sections separated by a diaphragm, which is often made of a polycarbonate or thin aluminum plate. One side is pressurized until the diaphragm bursts. The rapid expansion of gasses causes the formation of a shockwave that propagates through the lower pressure section. The high-pressure section is referred to as the driver section, and the low-pressure side, the one in which the shock wave propagates, is known as the driven section. Details are shown in Figure 1. The conditions in each of the shock-tube sections can be determined if the incident-shock velocity, V_i, is known by using the ideal gas approximation and the shockwave relations shown in equations (1) through (11).

Zone 1 is the gas before shock wave passage, Zone 2 is the gas behind the incident shock wave, and Zone 5 is the gas behind the reflected shock wave. The contact surface is the interface between the gasses that were in the driver and driven sections prior to the breaking of the diaphragm. When the diaphragm bursts, a shock wave travels ahead of the contact surface, eventually reflects off of the endwall, and then travels back the opposite direction resulting in the intersection of the contact surface and the shockwave.

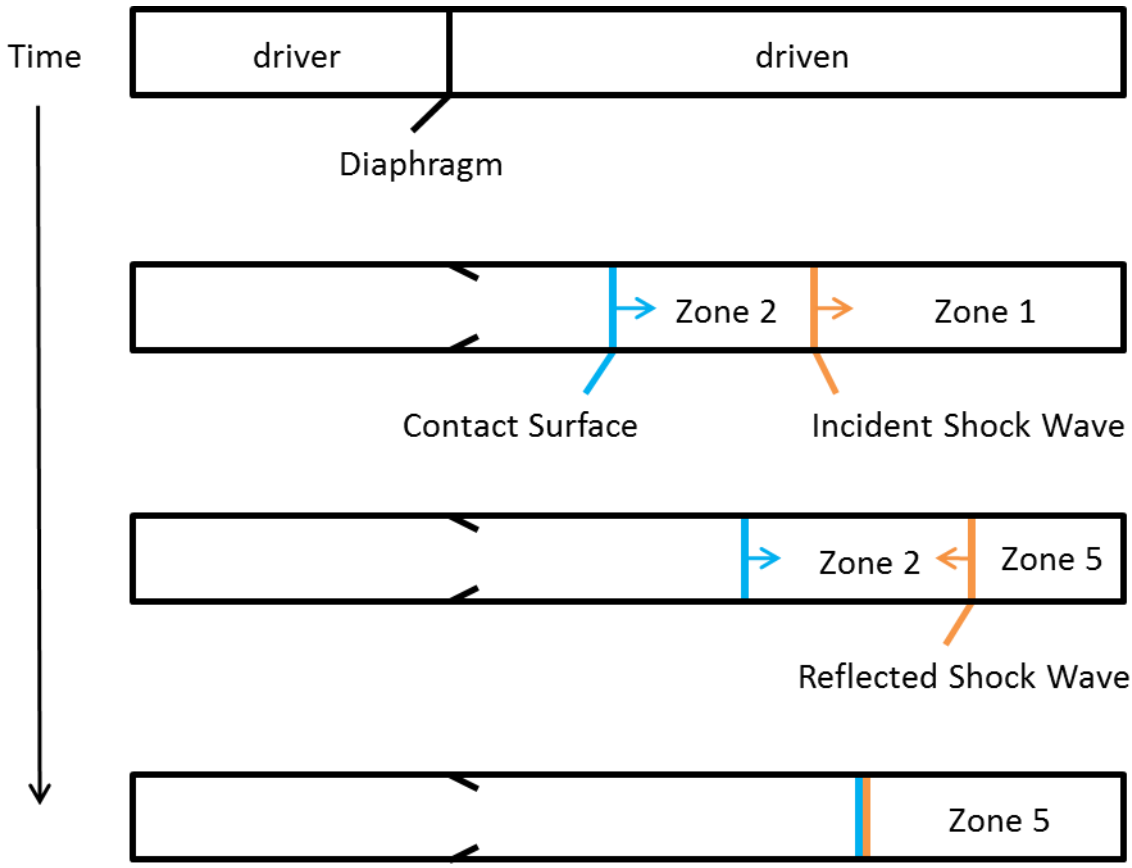

Figure 1. Diagram of shock tube physics.

$$a_1 = \sqrt{kRT_1} \tag{1}$$

$$M_i = \frac{V_i}{a_1} \tag{2}$$

$$\frac{P_2}{P_1} = \frac{2k}{k+1} M_i^2 - \frac{k-1}{k+1} \tag{3}$$

$$V_2 = V_i \left\{ \frac{2}{k+1} \left[1 - \left(\frac{a_1}{V_i} \right)^2 \right] \right\} \tag{4}$$

$$M_2 = \frac{V_2}{a_2} \tag{5}$$

$$\frac{T_2}{T_1} = 1 + \frac{k-1}{2a_1^2} (2V_i V_2 - V_2^2) \tag{6}$$

$$a_2 = \sqrt{kRT_2} \tag{7}$$

$$V_r = -V_2 - \left(\frac{a_2^2}{V_2 - M_i} \right) \tag{8}$$

$$\frac{P_5}{P_2} = \frac{2k}{k+1} \left(\frac{V_r + V_2}{a_2} \right)^2 - \frac{k-1}{k+1} \tag{9}$$

$$M_r = \frac{V_r + V_2}{a_2} \tag{10}$$

$$\frac{T_5}{T_2} = \frac{2(k-1)}{(k+1)^2} \left(\frac{1}{M_r^2} \right) \left(1 + \frac{k-1}{2} M_r^2 \right) \left(\frac{2k}{k-1} M_r^2 - 1 \right) \tag{11}$$

2.2 Special Considerations

A new test section was designed for the existing shock tube, and the previous test section was replaced. To simulate a wide range of shock strengths at real world conditions, the test section is designed to handle shock velocities up to Mach 2 with an initial pressure of 1 atm, and is capable of holding pressures up to 230 psi behind the reflected shock wave. Higher Mach numbers are achievable with initial pressures below 1 atm. Conditions behind the reflected shock wave determine the upper bounds on allowable

shock strength. The possibility of a dump tank being added in the future would allow even greater shock strengths if necessary.

The area of interest for dust layer-shock wave interaction is Zone 2, the gas behind the incident shockwave. The optimum test location is the one which allows for the longest observation time of Zone 2. The location within the shock tube where the contact surface and reflected shock intersect is where the longest possible observation time occurs, as this location spends the longest duration within Zone 2. The location varies with the shock strength because it is dependent on the shock velocity. This location was derived for a Mach 2 shock and 1 atm initial pressure using an x-t diagram shown in Figure 2 and is given by equation (12). Equation (13) gives the maximum observation time at a given test location. For the current facility, the test location at which the observation time is maximized is 3.33 meters from the diaphragm. It should be noted that observation time increases as Mach number decreases. At the selected test location, the predicted observation time for Mach 2 and Mach 1.3 shocks is 2.8 ms and 3.4 ms, respectively.

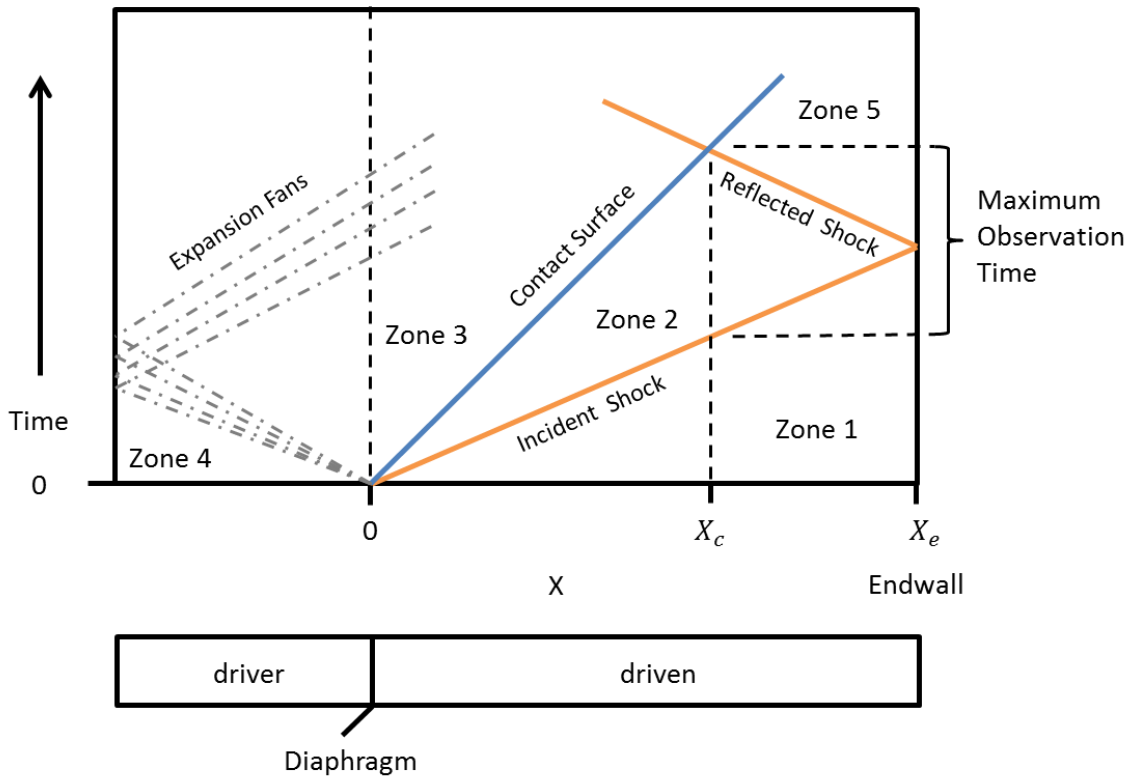

Figure 2. Shock tube x-t diagram. X = 0 is the location of the diaphragm, X_c is the location at which the longest observation time of Zone 2 occurs, X_e is the location of the endwall. Time = 0 is the time at which the diaphragm bursts and a shockwave is formed.

$$X_c = \frac{\frac{V_r}{V_i}+1}{\frac{V_r}{V_2}+1} X_e \tag{12}$$

$$t_{obs} = \frac{X_e - X_c}{V_i} + \frac{X_e - X_c}{V_r} \tag{13}$$

2.3 Design Specifications

2.3.1 Shock Tube Specifications

The shock-tube is constructed of 304 Stainless Steel with a round driver section and square driven section. The driver section is 7.6 cm in diameter and 1.5 meters in length. The driven section is approximately 10.8 × 10.8 cm and 3.9 meters long. The shock velocity is determined by a series of pressure transducers connected to three timing gates. Of the three timing intervals, one is before the dust layer test section, one spans the test section, and one is after the test section. The first pressure transducer is also used to trigger the camera to begin recording. Further details on the measurements are provided below. The shock-tube schematic with timers is shown in Figure 3. A detailed isometric view of the test section is shown in Figure 4.

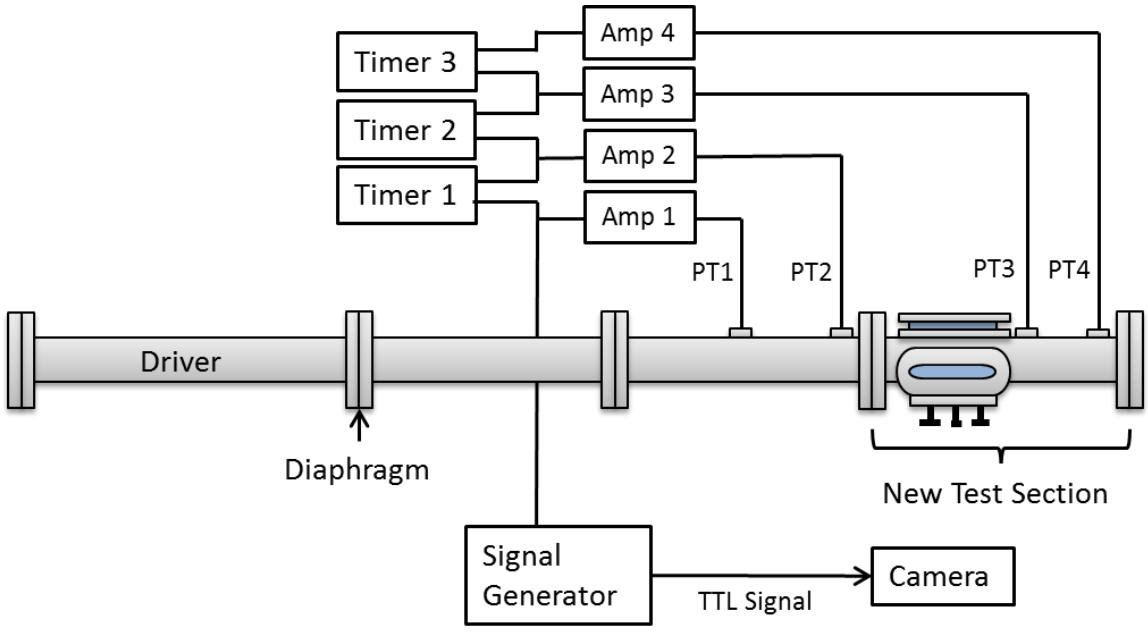

Figure 3. Schematic of shock tube layout, PT – Pressure Transducer

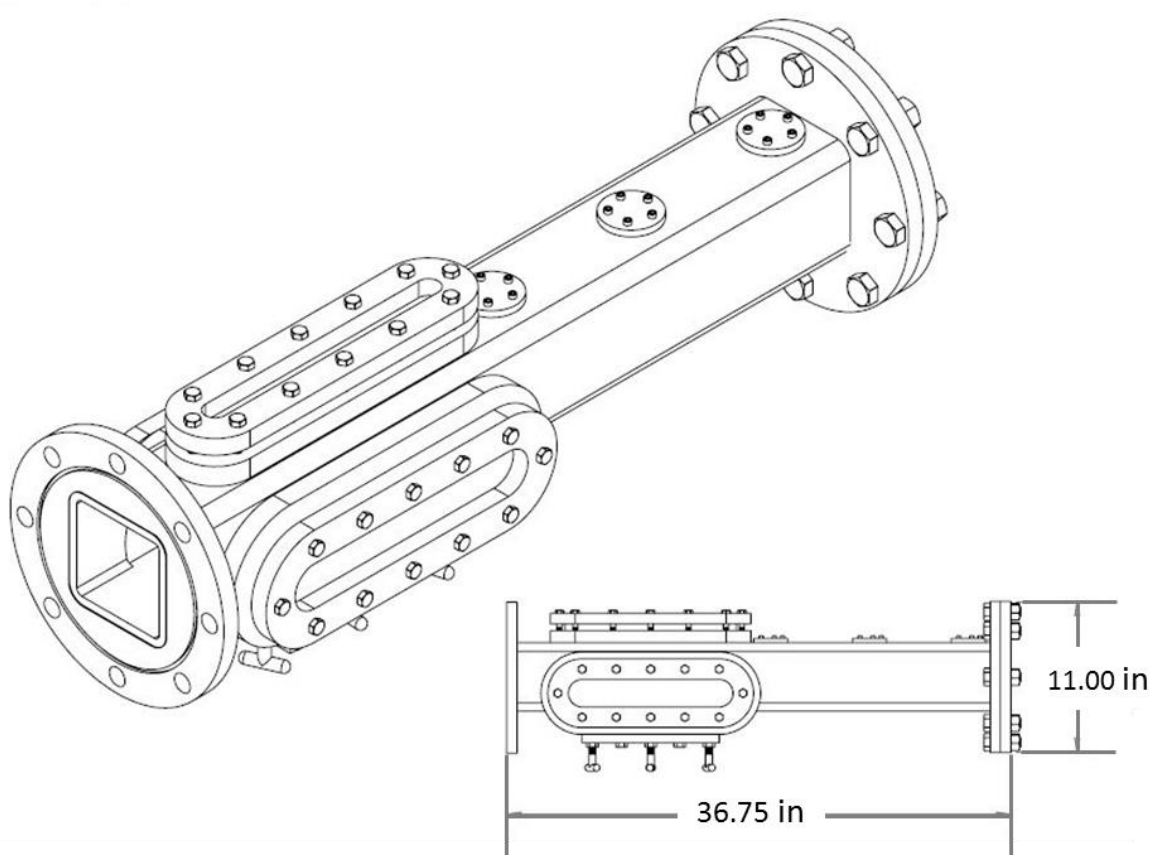

Figure 4. Isometric and side view of new test section.

2.3.2 Windows

The test section is comprised of obround windows on the top, left and right sides, and a dust pan on the bottom side. The left and right windows are each 2 by 12 inches and allow for viewing of the dust layer and fluid interface as well as for shadowgraph and schlieren techniques. The top window is 1 by 12 inches and allows for the future use of laser-sheet laser scattering techniques in which a laser-sheet is projected through the top window onto the test area, and scattering is observed through the side windows. The windows are rated up to 230 psi and were acquired from Archon Industries Inc. Stepped

window faces are used to keep the inside surface of the shock tube flush and limit disturbances of the flow field.

2.3.3 Dust Pan

Dust is placed in an easy-to-remove dust pan with a dust deposit area of 2.75 by 10.75 inches. The dust pan has four secure, removable inserts which allow for the adjustment of the dust layer thickness in 1/8-inch increments between 1/8 and 1/2 in. The dust pan was designed to be easily removable and is secured by six, T-handle, 1/2”-13 screws. The T-handles are threaded through 1/2-inch stainless steel plate which is secured to the shock tube window weld pads. The T-handles only need to be hand-tight to provide enough clamping force to secure the dust plate and provide a leak-tight seal. At maximum design pressure, the total force on the dust plate is approximately 4,300 lbs. Solidworks FEA analysis was used to determine optimum location of the T-handles to minimize deflection of the dust pan, which could cause leaks. The dust pan inserts are made from 1/8-inch-thick aluminum plate for its ease of fabrication. They are secured in place by two, 10-32 counter-sunk screws. The counter sink keeps the surface flat. Different-length screws are required for different dust layer thicknesses. Dust layer depths of 1/8, 1/4, 3/8 and 1/2 inches are possible with the present inserts, but shim stock could be used in addition to the current plates to make almost any depth possible up to 0.5 inches.

2.3.4 Vacuum Manifold

A separate vacuum manifold was designed to protect existing facility equipment from the negative effects of fine dust particles. The manifold is made up of 1/2- and 1/4-inch Swagelok tube and fittings. The section includes a roughing pump, exhaust vent, and analog and digital pressure measurements. The roughing pump is a Varian DS102 dual stage rotary vane vacuum pump. The inlet is 0.5 inches, and the outlet is 0.75 inches. The system takes five minutes to reach below five torr. An Omega PX309 pressure transducer, rated for up to 50 psi, was used. For pressures greater than 50 psi, an analog gauge is used with a scale up to 300 psi. The digital transducer allows for more accurate pressure readings during vacuuming and filling of the test section. A 0.25-in exhaust hose is used to vent the shock tube to the laboratory's exhaust ventilation system when the shock-tube pressure is above atmospheric pressure. Once the shock-tube pressure reaches atmospheric pressure, the vacuum pump is used to remove post-experiment gasses from the tube. A schematic of the shock-tube plumbing is shown in Figure 5.

Prior to an experiment, all filling of the shock tube is done through the pre-existing mixing manifold. Post experiment, all gasses are evacuated through a separate manifold to protect the mixing manifold from dust contamination. Only atmospheric air was used in this study, but the existing mixing manifold allows for the possibility of other gas mixtures.

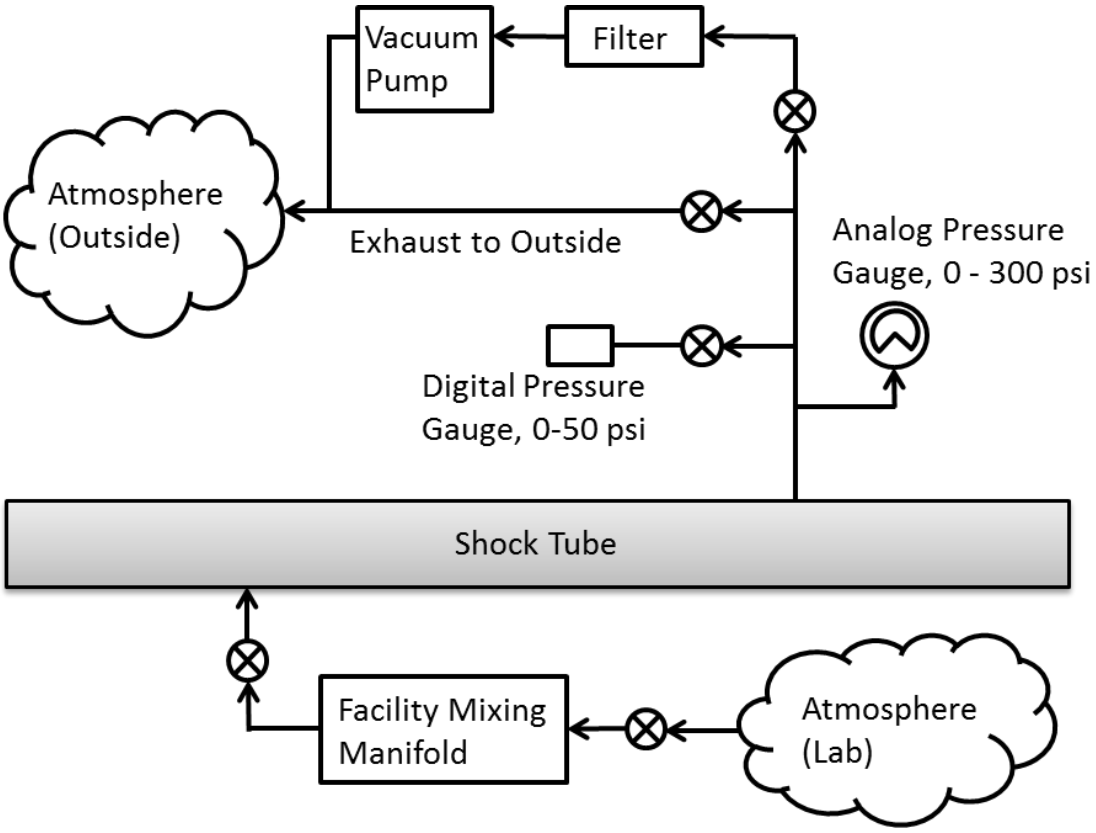

Figure 5. Shock tube plumbing schematic.

3. EXPERIMENTAL SETUP

3.1 Experimental Variables

Experimental variables include initial pressure, Mach number, dust layer thickness and characteristics of the dust itself. The pressure is controlled through the shock-tube's vacuum manifold, while the Mach number is altered by changing the diaphragms and driving-gas species. The initial pressure will also influence the Mach number. The dust and dust layer thickness are changed using a removable dust pan section with removable inserts. Thin, polycarbonate diaphragms are used with either Helium or Nitrogen as the driving gas. Initial tests were carried out with lime stone dust in air. Care must be taken to avoid dust particle combustion for potentially reactive dust species such as coal dust. When using potentially reactive dust, pure Nitrogen should be used as the driven gas because it is inert and has similar properties to air. In this study inert limestone dust was used with air.

3.2 Optical Arrangement

At the time of writing, the shadowgraph technique is solely employed for flow field visualization. The present experimental viewing area is approximately 76 mm wide by 50 mm high with the width being limited by the concave mirror diameter and height by the height of the window; larger-diameter, concave mirrors would allow for a wider viewing area. The curved mirrors have a 76-mm diameter and 17.5 inch focal length, resulting in an F# of 5.8. A Phototron high-speed camera at a frame rate of 15,000 fps is

used in conjunction with a Mercury Xenon 70-W lamp to capture the fluid and dust layer interaction. A schematic of the shadowgraph arrangement is shown in Figure 6.

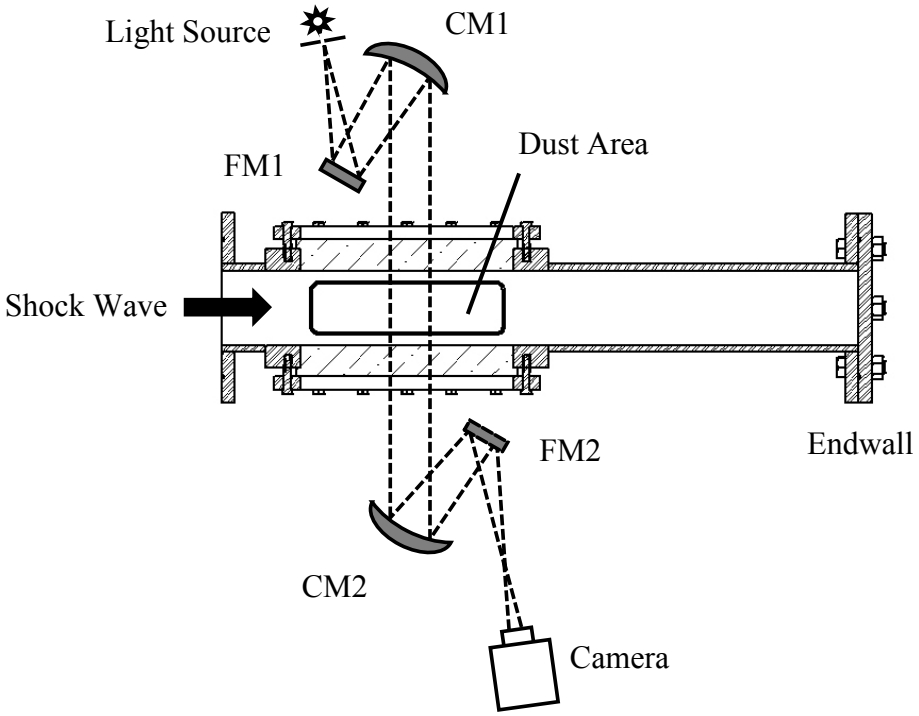

Figure 6. Schematic of shock-tube test section shadow graph arrangement. FM – Flat Mirror, CM – Curved Mirror

Particle lifting was measured with respect to shock-wave propagation. Dust rise was determined by examining the shadowgraph images. The corresponding shock wave propagation was derived from the shock velocity and time recorded by the camera using a known camera trigger location. Typical images are shown in Figure 7.

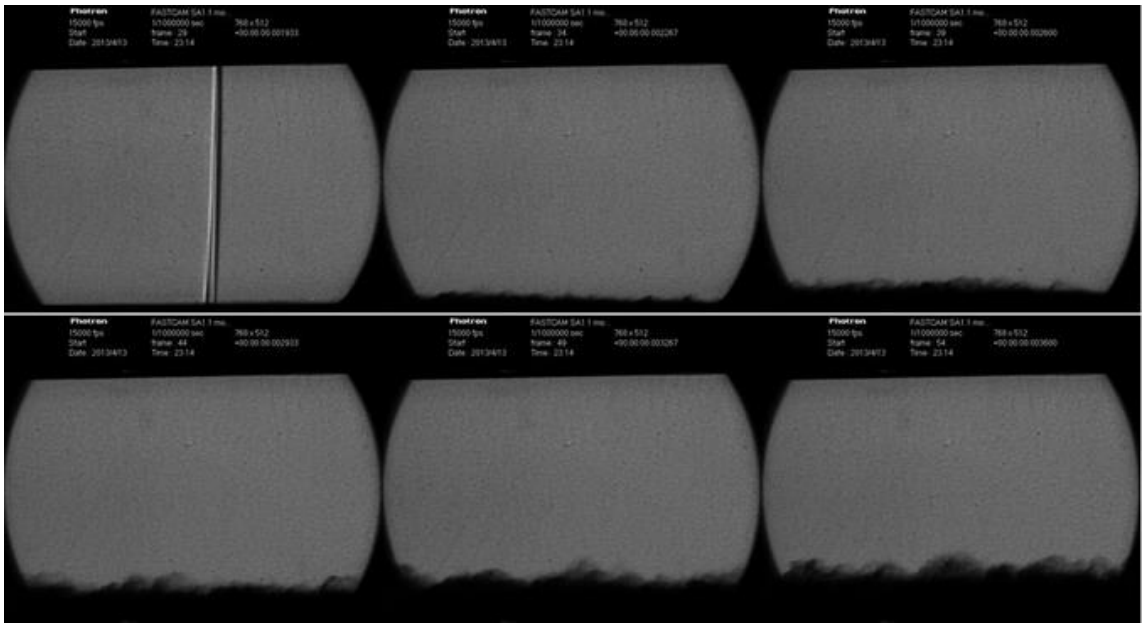

Figure 7. Images of air and limestone dust interaction in the flow behind a shock. M = 1.2, dust particle size = 40 µm, layer depth = 1/8 in, 15,000 frames per second, 1-µs exposure time. The time between each image is 333.3 µs.

3.3 Shock Wave Characterization

Prior to running dust experiments, a series of shocks were run to character the testing conditions and shock strength. Initial pressure, diaphragm thickness, and driving gas were changed and their influence on testing conditions monitored. Pressure varied from 100 to 500 torr, and diaphragm thicknesses between 0.005 and 0.020 inches were used. Both Helium and Nitrogen were tested as a driving gas. The Helium-driven shocks were stronger than desired, and Nitrogen was chosen as the driver gas for experiments. The preliminary runs also ensured all of the equipment was properly set up and allowed for the adjustment of timer sensitivity and camera settings. This procedure ensured target test conditions were accurate and repeatable prior to using any dust, which requires

cleaning of the shock tube after each experiment. Shock wave characterization data are shown in Table 1.

Table 1. Shock strength characterization test runs

Run #	Driver Gas	Diaphragm Thickness (in)	T_1 (K)	P_1 (torr)	Mach #
2593	Helium	0.005	295	100.0	1.96
2594	Helium	0.005	295	202.5	1.68
2595	Helium	0.005	295	299.9	1.54
2596	Helium	0.005	295	504.7	1.41
2599	Nitrogen	0.005	295	100.0	1.61
2600	Nitrogen	0.005	295	100.0	1.62
2601	Nitrogen	0.005	295	100.0	1.61
2602	Nitrogen	0.005	295	499.7	1.22
2603	Nitrogen	0.010	295	499.7	1.36
2604	Nitrogen	0.015	295	500.0	1.42
2605	Nitrogen	0.020	295	500.0	1.47
2607	Nitrogen	0.020	295	300.2	1.53
2608	Nitrogen	0.005	295	500.1	1.24
2609	Nitrogen	0.005	295	500.8	1.37
2610	Nitrogen	0.005	295	500.3	1.24
2611	Nitrogen	0.015	295	500.0	1.38
2612	Nitrogen	0.015	295	500.2	1.30

3.4 Procedure

To test the new facility, the effect of shock strength on the dust layer was chosen for study as it allows for easy comparison to trends presented in the literature. Using 40-μm limestone dust and a 1/8-in thick layer, shock strength was varied using Mach numbers of approximately 1.23 and 1.38. The initial pressure was kept constant, and only the diaphragm was altered to vary the Mach number. The driver gas was Nitrogen. 0.005-in

and 0.020-in thick polycarbonate diaphragms were used to obtain the Mach 1.23 and 1.38 shock strengths, respectively. Three runs were done at each condition to ensure repeatability. The test conditions are shown in Table 2.

Table 2. Dusty shock experiment conditions at which data were collected.

Run #	Driver Gas	Diaphragm Thickness (in)	T_1 (K)	P_1 (torr)	Mach #
2613	Nitrogen	0.005	295	500.1	1.23
2614	Nitrogen	0.005	295	500.1	1.23
2615	Nitrogen	0.005	295	500.0	1.23
2616	Nitrogen	0.020	295	500.2	1.35
2617	Nitrogen	0.020	295	500.0	1.38
2618	Nitrogen	0.020	295	500.0	1.39

Test procedures begin with a clean shock tube open at the diaphragm loading access point and with all valves connecting to the shock tube closed. The following steps were followed when running experiments.

1. Remove dust pan from shock tube and set to the appropriate layer depth.
2. Add uniform flat dust layer to dust pan taking care to minimize compaction.
3. Replace dust pan back into shock tube and tighten.
4. Install desired diaphragm into breech loader and tighten. At this point, the shock tube should be fully sealed and the driver and driven section separated by the diaphragm.
5. Simultaneously vacuum down the driver and driven sections.

6. Once the driver section has fallen below 5 torr, stop vacuuming the driver section, and using the mixing manifold, fill the driver section with air from the atmosphere to the desired pressure (the initial experiment pressure, P_1).
7. Once the desired P_1 is reached, stop filling and make sure that all lines connecting to the driven section are closed.
8. Check that the timers are properly set and awaiting an input, reset them if necessary.
9. Check that the light source is on and set to 70 Watts, if it is off, turn it on.
10. Check that the camera is on and ready to record, if it is off, turn it on.
11. Check that the camera trigger switch is on and ready, if it is off, turn it on.
12. After all data recording equipment is on and ready to receive to input, stop vacuuming the driver section, and fill with Nitrogen until the diaphragm bursts.
13. Once diaphragm bursts, close the fill valve.
14. Record the counter times and reset the counters.
15. Crop camera recording and save in .avi and .bmp file formats.
16. Turn off the camera and light source.
17. Before preparing the shock tube for the next experiment, allow at least ten minutes to pass for the agitated dust to settle.
18. Using analog pressure gauge on the test section exhaust manifold, note the equilibrium pressure inside of the shock tube, if the pressure is below 50 psi, the digital pressure gauge may be used to monitor pressure.

19. If the shock-tube pressure is above 1 atm, vent the gas through the exhaust ventilation, otherwise, continue to the next step.
20. Once the shock-tube pressure is at or below 1 atm, vacuum the shock tube to below 5 torr using the exhaust manifold to remove the previous test gases and any remaining suspended dust particles.
21. Once the previous test gases have been evacuated, stop vacuuming, and fill the shock tube with atmospheric air until it reaches an equilibrium with the room pressure.
22. Open the shock tube at the diaphragm breech loader and remove the used diaphragm, inspect for improper break which could influence test results.
23. Remove the endwall from the shock tube and using a portable shop vacuum, remove as much of the dust as possible.
24. After vacuuming the dust, use brush on the end of long telescoping pole to remove dust deposits from the shock tube walls, and brush as much as possible towards the endwall of the shock tube.
25. Using a portable shop vacuum, vacuum the interior of the shock tube a second time removing as much dust from the previous experiment as possible.
26. Remove the dust pan from the shock tube.
27. Using a cloth or paper towel and acetone, clean off the dust deposits from the interior and exterior of the windows. The 1/2” plate which supports the dust pan may need to be removed to gain access to the interior of the windows. Remove it and reinstall it afterwards if necessary.

28. Reinstall the endwall.
29. The shock tube is now ready for the next experiment with the dust pan removed.

    Repeat the procedure form step 2 for the next experiment.

3.4.1 Dust Preparation

Special care must be taken when preparing the dust prior to experiments as differences in this procedure could show up in the data. For this study, 40-μm limestone dust was used. The dust had a strong tendency to agglomerate which increased the difficulty of making a uniform, flat dust layer. To overcome this obstacle, much more dust was initially added to the dust pan than would be used in experiment. The dust pan cavity was filled with dust until it was overflowing from the top. A piece of paper was then dragged across the top of the edge of the dust plate at an angle just above and parallel with the plate. This technique effectively cut through the large agglomerates and resulted in the least amount of disturbance of the dust within the cavity. Agglomerates had a tendency to drag the dust particles below them resulting in a non-uniform distribution. To overcome this result, the process of adding dust and cutting off the top was repeated until a uniform dust layer was achieved. A straightedge was initially used but was less effective as it would grab and pull conglomerates. The paper had the effect of cutting through these instead of dragging them, reducing the disturbance of the dust layer cavity and resulting in a more-uniform dust layer. Care was taken to minimize compaction of the layer during this process.

3.4.2 Image Processing

The bitmap images that were taken during experiments were analyzed frame by frame. A user-created MATlab add-on application, Image Measurement Utility created by Jan Neggers, was used to process the images (application available at http://www.mathworks.com/matlabcentral/fileexchange/25964-image-measurement-utility/content/Image%20Measurement%20Utility.mlappinstall). To calibrate the image measurements, a calibration image was taken using a pair of digital calipers opened to 10.00 mm. A calibration line was draw between the measuring edges of the calipers and the corresponding 10.00 mm value entered into the program. Once this procedure was done, point-to-point measurements could be accurately taken. Lines drawn using the utility would remain visible even if a new image was selected. This result allowed for convenient use of reference lines that did not need to be re-drawn for each new image. The x-location chosen as the point of reference for measurements was the 384th pixel on the x-axis of the image. The image resolution was 768 by 576, and the 384th pixel is adjacent to the image centerline. Figure 8 shows the calibration and measurement of the images. When plotting the data, X_0 is the image centerline, and time zero is the time when the shock is at X_0.

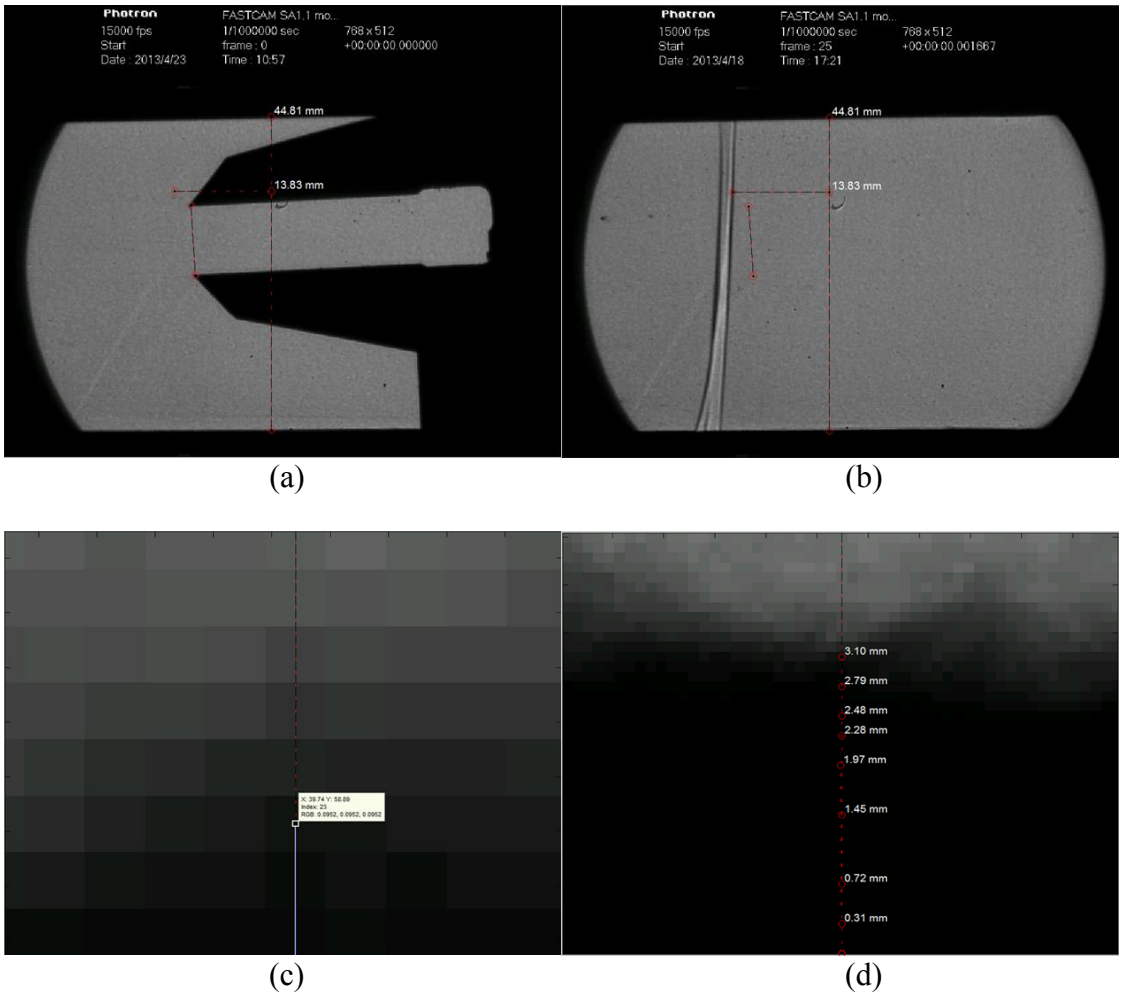

Figure 8. MATLab Image Measurement Utility calibration and determination of reference time zero. (a) calibration image, caliper opened to 10.00 mm; (b) measurement of observable height and distance of shock wave from viewing centerline; (c) zoomed in view of pixel grid for finding RGB threshold; (d) dust boundary measurement with measurements from previous frames present

The edge of the dust layer cloud was defined using the pixel red, green, and blue (RGB) intensity. Because the images are greyscale, this value was the same for red, green and blue. Boundaries were evident when RGB intensity was below 0.100, and this value was chosen as the threshold for defining the edge of dust cloud boundary. At longer observation times, a background dust cloud would enter the observation area, increasing

the uncertainty. This cloud is caused by residual dust deposits on the shock-tube walls from previous experiments being lifted and carried into the observation area. Once this background dust cloud entered the frames, the 0.100 threshold was no longer sufficient to distinguish a zone that contained dust from the initial layer, or one that consisted of the background cloud. To overcome this difficulty, after the appearance of the background dust cloud, a RGB threshold of less than 0.0300 was used. This adjustment provided an accurate representation of the boundary between areas that were filled with dust lifted from the initial dust layer, and those which were composed of background dust. The background dust cloud can be observed in Figure 9. Note that a boundary is still evident between the background and dust which was lifted from the dust layer despite the presence of the cloud. Shifting from a RGB threshold of 0.10 to 0.03 to define the dust-lifting boundary allowed for greater accuracy in defining the boundary in the presence of the background cloud.

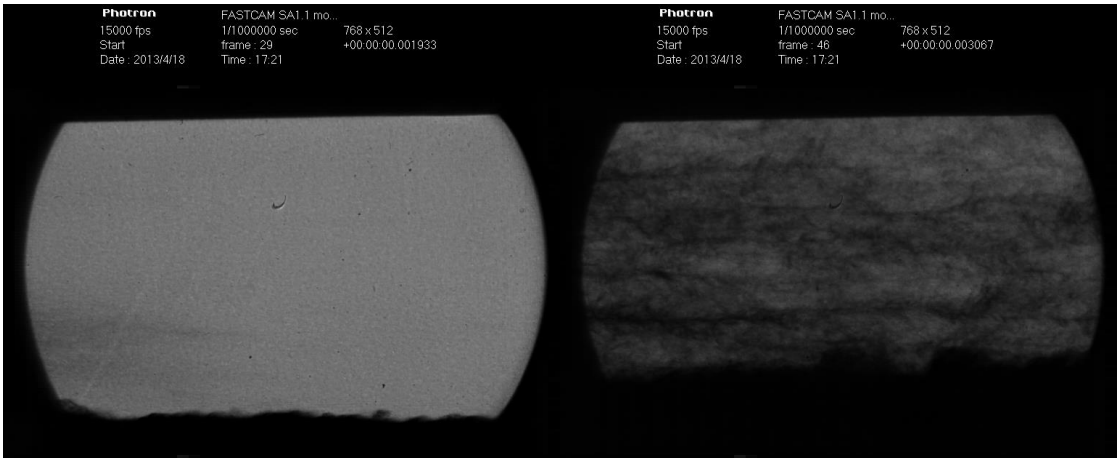

Figure 9. Comparison of images with and without the presence of a background dust cloud. Notice that the dust layer boundary is still visible, left – background cloud absent, right – background cloud present

4. RESULTS

4.1 Dust Particle Rise

Data were plotted in terms of dust particle rise with respect to shock wave propagation beyond the reference location at which particle height measurements were taken. Six graphs were made. Mach 1.22 and 1.37 data were plotted separately, and individual runs at those conditions were compared to check repeatability. All data were then plotted together on the same graph to compare the effect of shock strength on the dust particle rise height. The graphs are shown in Figures 10, 11, 12, and 13.

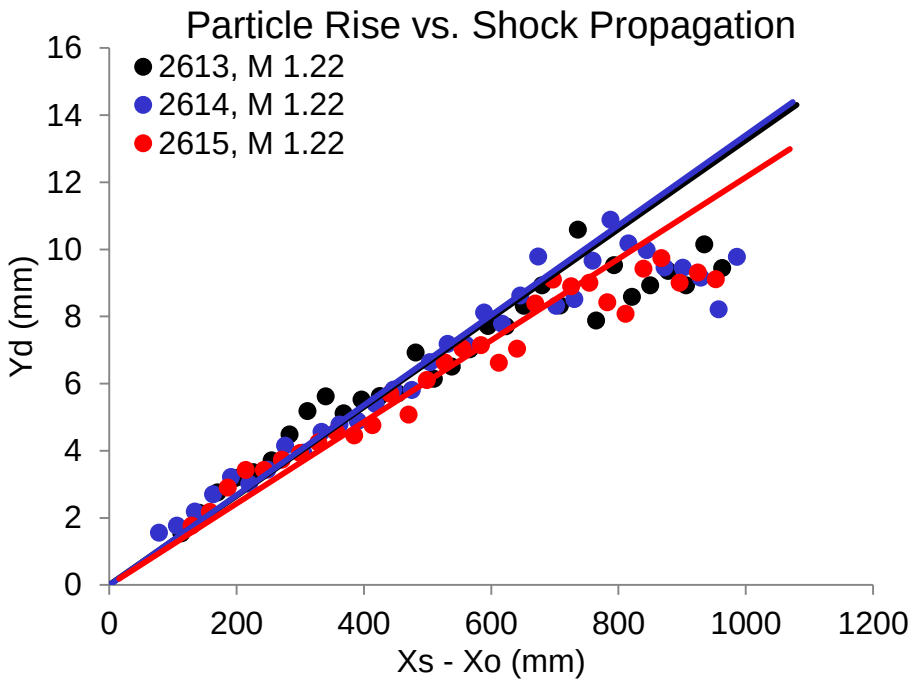

Figure 10. Mach 1.22 data for run numbers 2613, 2614, and 2615

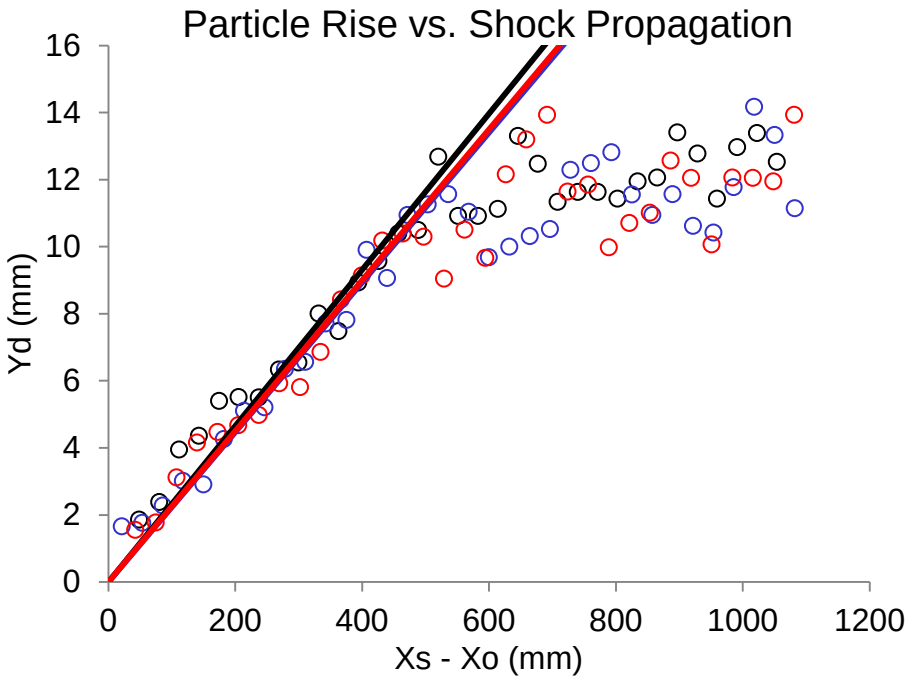

Figure 11. Mach 1.37 data for run numbers 2616, 2617 and 2618

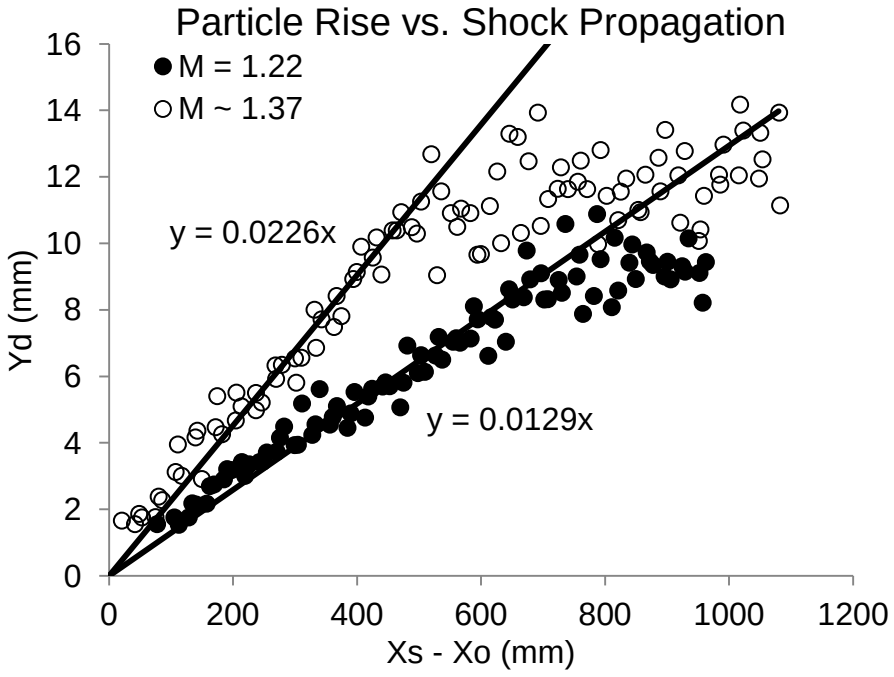

Figure 12. Dust rise height for Mach 1.22 and Mach ~1.37 shock waves.

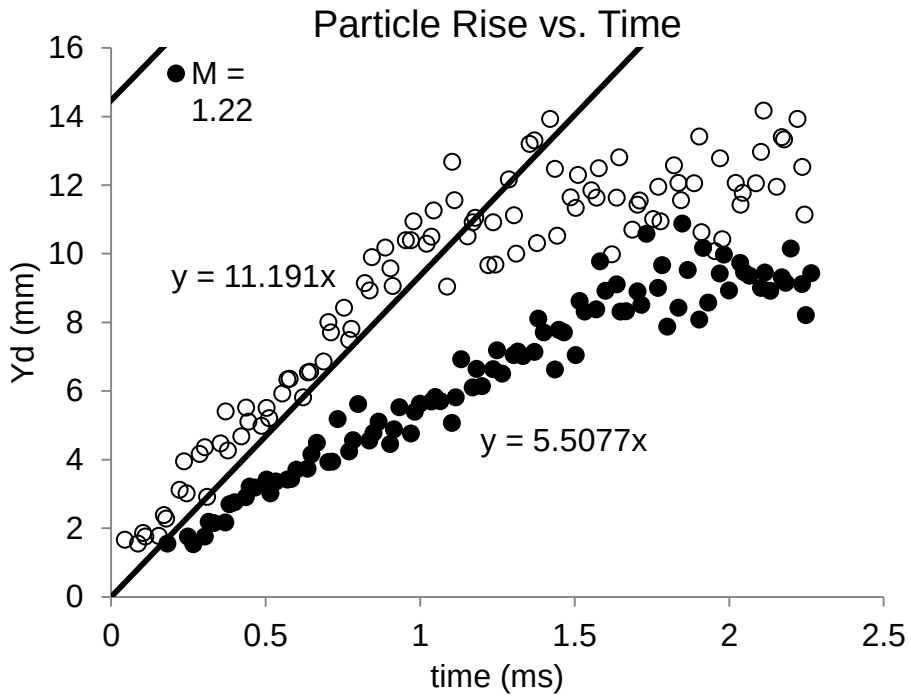

Figure 13. Dust particle rise vs. time.

4.2 Discussion

The data shows high repeatability from test to test. From MATlab, the dust layer cloud boundary can be discerned within +/- 0.3 mm. Other factors adding to the uncertainty include the dust erosion. As the time passes, more and more dust is removed from the dust layer, and the surface level changes. Slight differences in the manner in which the diaphragm breaks from one experiment to the other can also be responsible for slight differences in the shock front that can be difficult to characterize. In some cases, there are slight variations in shock strength. The differences in the dust layer between experiments also contributes to difficulty in achieving high repeatability as dust

agglomerate distribution can vary between dust layers prepared for different experimental runs, and this uncertainty is difficult to quantify. Despite these factors, the results presented show high precision in repeatability.

It is seen from the data that the shock strength plays a large role in the dispersion of dust particles behind a shockwave. It is also observed that dust particles behind a strong shock are lifted higher than those behind a weaker shock, and rise at a greater rate. A significant increase in the scatter of the data is observed at later times, and it is also evident that scatter in the data occurs more quickly with a stronger shock. The increased scatter at later times is observed for both shock strengths and is suspected to be caused by the onset of turbulence behind the shock wave. At later times (1 to 1.5 ms), the interface between the dust layer cloud and the fluid field resembles waves, similar in nature to those associated with Kelvin-Hemholtz instability. Examples are shown in Figure 14.

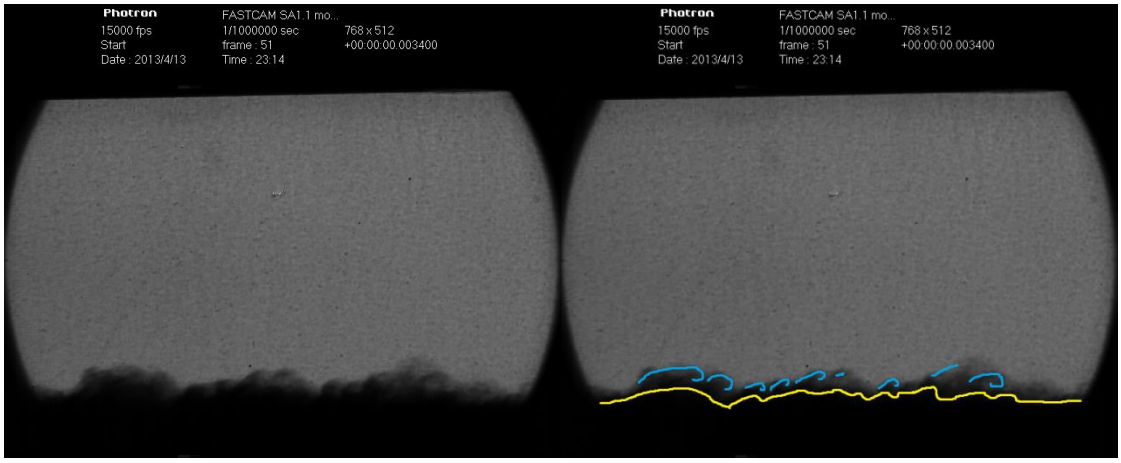

(a)

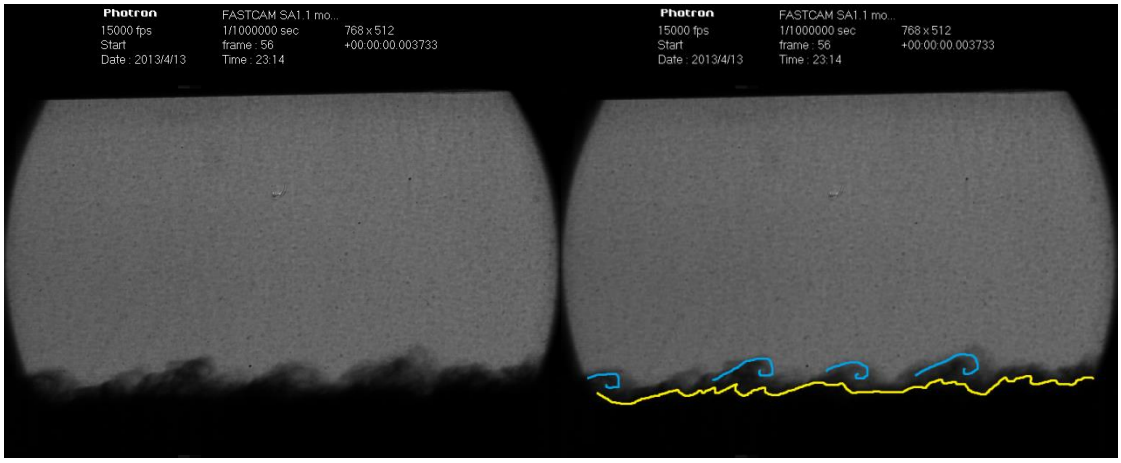

(b)

Figure 14. Example of wave-like boundary of dust layer. Left side raw image, right side outline of boundary and wave-like crests, Run 2613, M = 1.23, (a) frame 51 (b) frame 56

Hwang observed the onset of turbulence, but investigation of the phenomenon as it relates to dust layers, and multi-phase flow involving dusty gasses, appears limited (Hwang, 1982). Much attention has been given to the process of dust entrainment immediately after the passage of the shockwave, and less to the flow characteristics at longer time scales at which numerical models of entrainment mechanisms may no longer

be valid. In 1986, Hwang developed a model for the initial stages dust layer and shock wave interaction, and while he concluded the model showed good agreement with experimental measurements, he noted that the model was only valid as long as the boundary layer behind the shock wave remained laminar, and only for time durations less than 2 ms after shock wave passage across the dust layer (Hwang, 1986). While more recent models have been developed that, in general, show good agreement with experimental data, these models were verified with data obtained prior to the onset of increased turbulence observed herein, and the time duration for which these models are valid is not clearly stated.

4.3 Recommendations

In light of the observations made herein, further investigation of the development of turbulence at later times after the passage of the shock wave over the dusty layer is suggested. More experiments at different Mach numbers and the development of a correlation between the Mach number and dust layer rise are recommended. Also, the development of a method to determine the dust volumetric number density and mass density distribution within the rising dust cloud is also suggested because of its usefulness in the validation of theoretical models. Correlation between the onset of data scatter and flow turbulence requires further investigation, and it may be beneficial to study the transition of the dust layer from a homogeneous, bulk granular medium into a dusty gas as particles are lifted and dust erosion occurs. The time durations for which data were collected in the existing body of works, in general, were shorter than those

presented, and the investigation of flow instabilities in flow behind the shockwave is limited.

5. SUMMARY

A new shock-tube test section was developed and integrated into an existing shock-tube facility. The test section allows for shadowgraph or laser scattering techniques to track dust layer particle motion. The test section is designed to handle an initial pressure of 1 atm with an incident shock wave velocity up to Mach 2 to mimic real-world conditions. The test section features an easily removable dust pan and inserts to allow for adjustment of dust layer thickness. The design allows for the changing of experimental variables including initial pressure, Mach number, dust layer thickness and characteristics of the dust itself. A separate vacuum manifold was designed to protect existing equipment from negative side effects of the dust. A study was performed to demonstrate the capabilities of the new facility and to compare results with experimental trends formerly established in the literature. Dust layer rise height was graphed with respect to shockwave propagation. Dust particles subjected to a Mach 1.38 shock wave rose more rapidly and to a greater height with respect to shock wave propagation than particles subjected to a Mach 1.22 shock wave. These results are in agreement with trends found in the literature. An increase in the scatter of the data at later times (greater than 1 ms) and the appearance of flow boundaries that resemble those cause by flow instabilities were discovered. The data available in the literature for the observed time durations herein is scarce. The appearance of increased scatter within the data, development of flow instabilities at longer times than has been previously investigated are recommended as topics for future study.

REFERENCES

Abbasi, T. & Abbasi, S. A., 2007. Dust explosions - cases, causes, consequences, and control. *Journal of Hazardous Materials,* Volume 140, pp. 7-44.

Boiko, V. M. & Papyrin, A. N., 1987. Dynamics of the formation of a gas suspension behind a shock wave sliding over the surface of a loose material. *Combustion, Explosion, and Shock Waves,* 23(2), pp. 231-235.

Bracht, K. & Merzkirch, W., 1979. Dust entrainment in a shock-induced turbulent air flow. *Internation Journal of Multiphase Flow,* Volume 5, pp. 301-312.

Fan, B. C., Chen, Z. H., Jiang, X. H. & Li, H. Z., 2007. Interaction of a shock wave with a loose dusty bulk layer. *Shock Waves,* Volume 16, pp. 197-187.

Fedorov, A. V., 2004. Mixing in wave processes propagationg in gas mixtures (review). *Combustion, Explosion, and Shock Waves,* Volume 40, pp. 17-31.

Fedorov, A. V. & Fedorchenko, I. A., 2005. Computation of dust lifting behind a shockwave sliding along the layer. Verification of the model. *Combustion, Explosions, and Shock Waves,* 41(3), pp. 36-345.

Fletcher, B., 1963. The interaction of a shock with a dust deposit. *Journal of Physics D: Applied Physics,* Volume 14, pp. 186-192.

Gerrard, J. H., 1963. An experimental investigation of the initail stages of the dispersion of dust by shock waves. *British Journal of Applied Physics,* Volume 14, pp. 186-192.

Gidaspow, D., 1994. *Multiphase flow and fluidization.* San Diego: Academic Press.

Hwang, C. C., 1982. Interaction of a coal dust-bed with shock induced air stream. *Flow Visualization II,* pp. 547-551.

Hwang, C. C., 1986. Initial stages of the interaction of a shock wave with a dust deposit. *International Journal of Multiphase Flow,* 12(4), pp. 655-666.

Ilea, C. G., Kosinkski, P. & Hoffmann, A. C., 2009. The effect of polydispersity on dust lifting behind shock waves. *Powder Technology,* Volume 196, pp. 194-201.

Klemens, R., Zydak, P., Kaluzny, M., Litwin, D. & Wolanski, P., 2006. Dynamics of dust dispersion from the layer behinds the propagation shock wave. *Journal of Loss Prevention in Process Industries,* Volume 19, pp. 200-209.

Kuhl, A. L., Chien, K. Y., Ferguson, R. E., Collins, J. P. & Glaz, H. M., 1990. Simulation of a turbulent, dusty boundary layer behind a shock. *American Institue of Physics Conference Proceedings* Bethlehem, PA, American Institute of Physics, pp. 762-769.

Merzkirch, W. & Bracht, K., 1978. The erosion of dust by a shock wave in air: initial stages with laminar flow. *International Journal of Multiphase Flow,* Volume 4, pp. 89-95.

Skjold, T., Eckhoff, R. K., Arntzen, B. J., Lebechi, K., Dyduch, Z., Klemens, R. & Zydack, P., 2007. Simplified modeling of explosion propagation by dust explosion in coal mines. *Proceedings of the 5th International Seminar on Fire and Explosion Hazards*, Edinburgh, UK, School of Engineering and Electronics, University of Edinburgh, pp. 23-27.

Suzuki, T. & Adachi, T., 1984. The effects of particle size on shock wave dust deposit interaction. *International Symposium on Space Technology and Science*, Tokyo, AGNE Publishing, Inc., pp. 483-490.

APPENDIX A

TEST SECTION ENGINEERING DRAWINGS

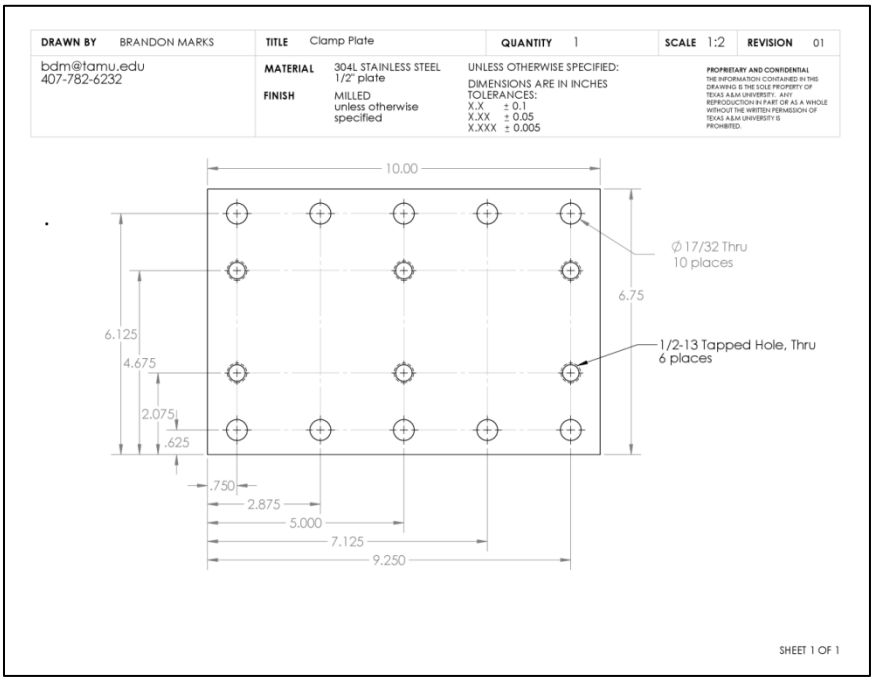

Figure A1. Dust pan clamping plate drawing. This plate is fixed to the window weld pads and secures the T-handles that clamp the dust pan into place.

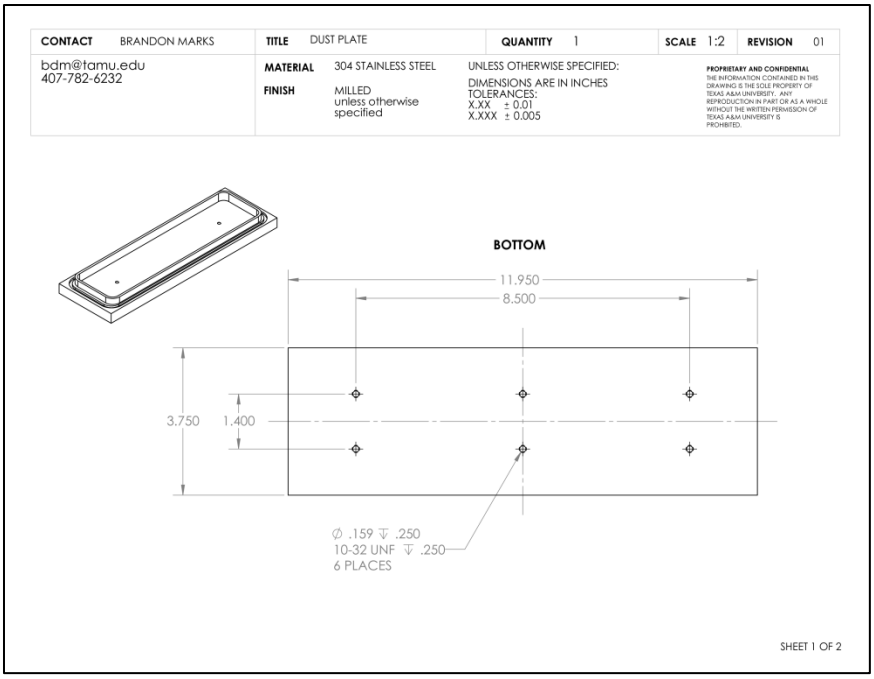

Figure A2. Dust pan drawing

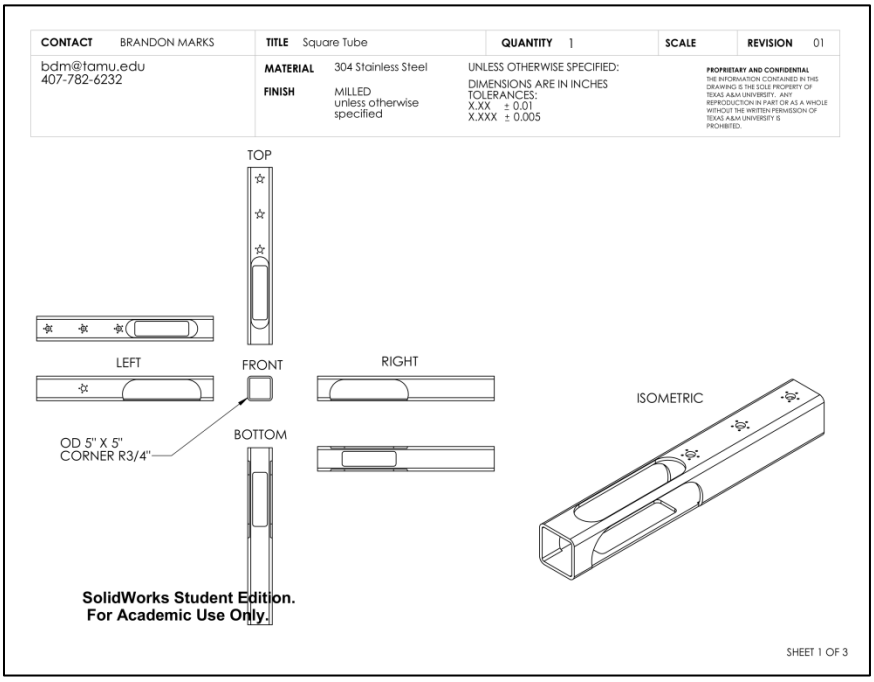

(a)

Figure A3. Square tube section drawing. (a) reference views (b) right and bottom detailed view (c) left and top detailed view

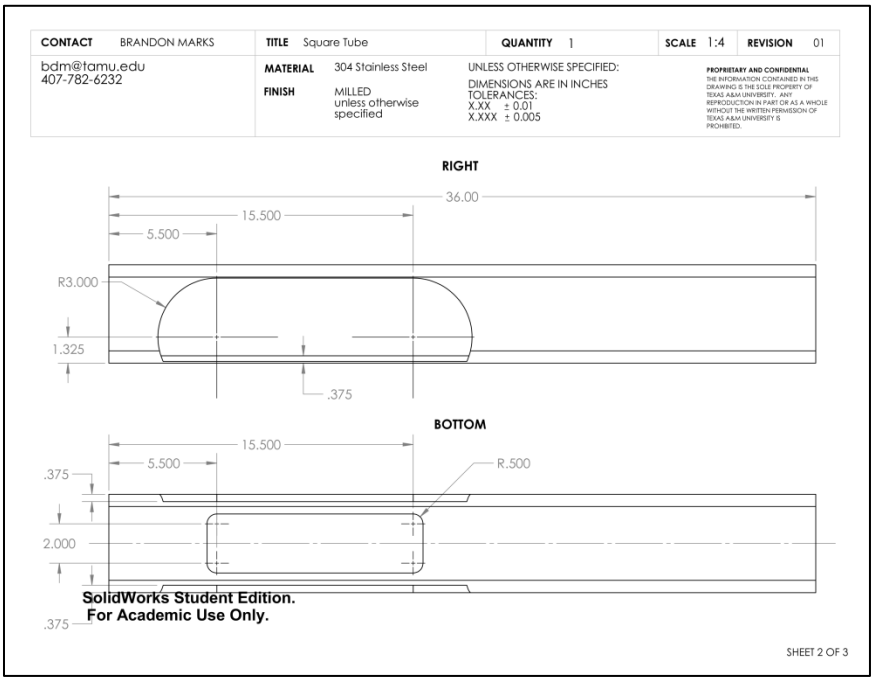

(b)

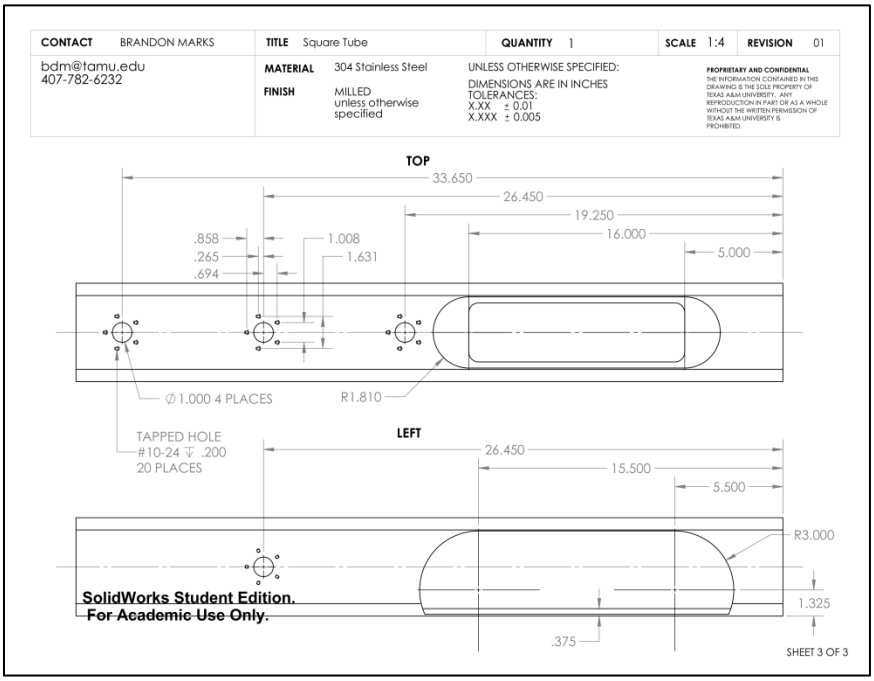

(c)

Figure A3. Continued.

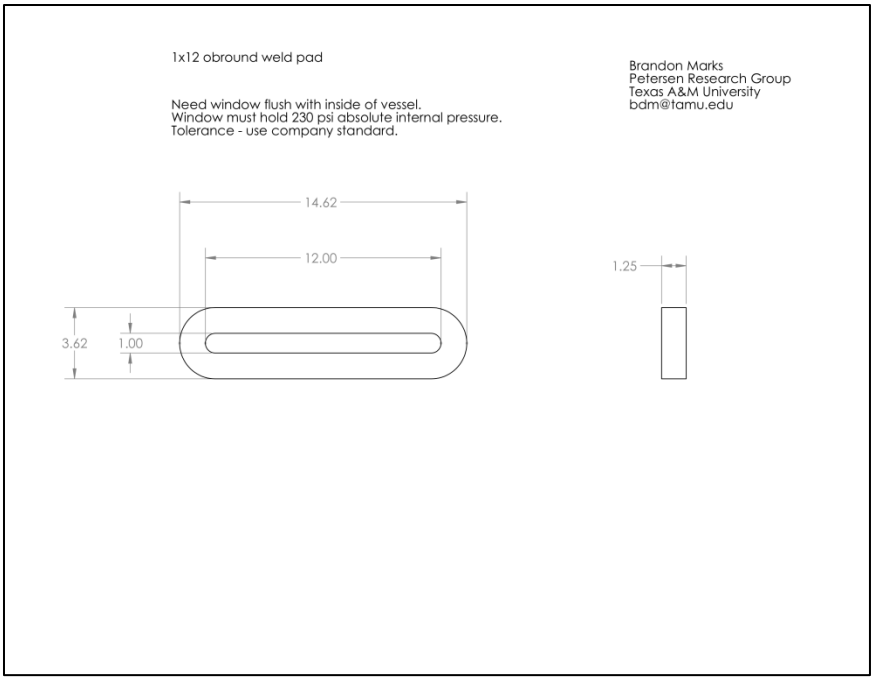

(a)

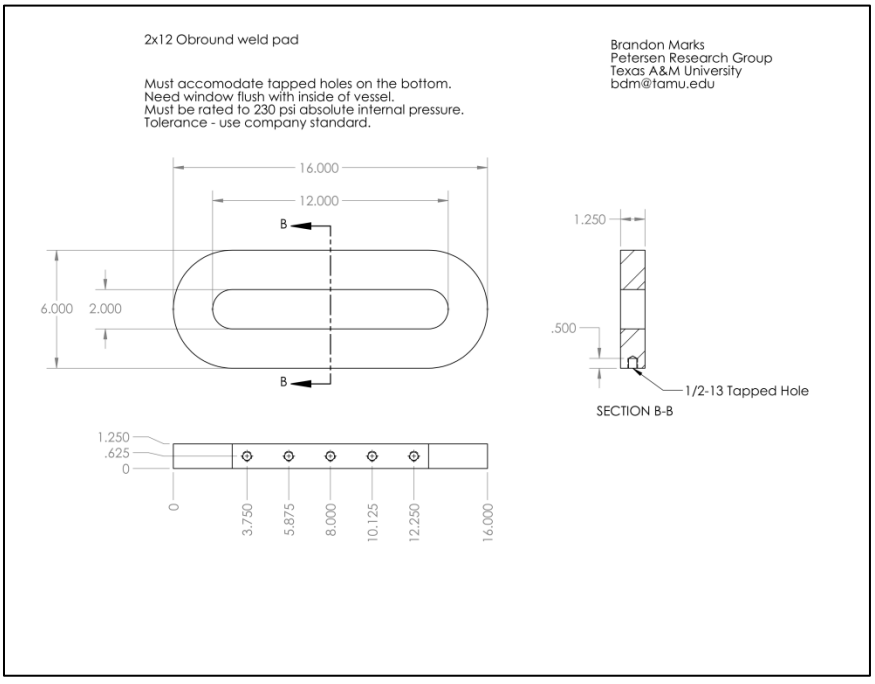

(b)

Figure A4. Window custom weld pad drawings supplied to Archon Industries Inc. (a) top window pad (b) side window pad

APPENDIX B

POST PROCESSED IMAGE DATA

Table B1. Experimental data Run 2613, M = 1.23

Run 2613, M = 1.23				
Frame	**Capture Time (s)**	**Time after shock passage (ms)**	**Shock Front Propagation, Xs - Xo (mm)**	**Dust Layer Height, Yd (mm)**
28	0.001867	0.000	0.0	
29	0.001933	0.066	28.0	
30	0.002000	0.133	56.5	
31	0.002067	0.200	85.0	
32	0.002133	0.266	113.0	1.5
33	0.002200	0.333	141.5	2.1
34	0.002267	0.400	170.0	2.8
35	0.002333	0.466	198.0	3.2
36	0.002400	0.533	226.5	3.4
37	0.002467	0.600	254.9	3.7
38	0.002533	0.666	283.0	4.5
39	0.002600	0.733	311.5	5.2
40	0.002667	0.800	339.9	5.6
41	0.002733	0.866	368.0	5.1
42	0.002800	0.933	396.4	5.5
43	0.002867	1.000	424.9	5.6
44	0.002933	1.066	453.0	5.7
45	0.003000	1.133	481.4	6.9
46	0.003067	1.200	509.9	6.1
47	0.003133	1.266	537.9	6.5
48	0.003200	1.333	566.4	7.0
49	0.003267	1.400	594.9	7.7
50	0.003333	1.466	622.9	7.7
51	0.003400	1.533	651.4	8.3
52	0.003467	1.600	679.9	8.9
53	0.003533	1.666	707.9	8.3
54	0.003600	1.733	736.4	10.6
55	0.003667	1.800	764.8	7.9
56	0.003733	1.866	792.9	9.5
57	0.003800	1.933	821.4	8.6
58	0.003867	2.000	849.8	8.9
59	0.003933	2.066	877.9	9.4
60	0.004000	2.133	906.3	8.9
61	0.004067	2.200	934.8	10.1
62	0.004133	2.266	962.8	9.4

Table B2. Experimental data Run 2614, M = 1.23

Run 2614, M = 1.23				
Frame	**Capture Time (s)**	**Time after shock passage (ms)**	**Shock Front Propagation, Xs - Xo (mm)**	**Dust Layer Height, Yd (mm)**
28	0.001867	0.000		
29	0.001933	0.049	20.8	
30	0.002000	0.116	49.4	
31	0.002067	0.183	77.9	1.6
32	0.002133	0.249	106.0	1.8
33	0.002200	0.316	134.5	2.2
34	0.002267	0.383	163.0	2.7
35	0.002333	0.449	191.1	3.2
36	0.002400	0.516	219.7	3.0
37	0.002467	0.583	248.2	3.4
38	0.002533	0.649	276.3	4.2
39	0.002600	0.716	304.8	3.9
40	0.002667	0.783	333.4	4.6
41	0.002733	0.849	361.5	4.8
42	0.002800	0.916	390.0	4.9
43	0.002867	0.983	418.5	5.4
44	0.002933	1.049	446.6	5.8
45	0.003000	1.116	475.1	5.8
46	0.003067	1.183	503.7	6.6
47	0.003133	1.249	531.8	7.2
48	0.003200	1.316	560.3	7.2
49	0.003267	1.383	588.8	8.1
50	0.003333	1.449	616.9	7.8
51	0.003400	1.516	645.5	8.6
52	0.003467	1.583	674.0	9.8
53	0.003533	1.649	702.1	8.3
54	0.003600	1.716	730.6	8.5
55	0.003667	1.783	759.1	9.7
56	0.003733	1.849	787.2	10.9
57	0.003800	1.916	815.8	10.2
58	0.003867	1.983	844.3	10.0
59	0.003933	2.049	872.4	9.5
60	0.004000	2.116	900.9	9.5
61	0.004067	2.183	929.4	9.2
62	0.004133	2.249	957.5	8.2

Table B3. Experimental data Run 2615, M = 1.23

Run 2615, M = 1.23				
Frame	**Capture Time (s)**	**Time after shock passage (ms)**	**Shock Front Propagation, Xs - Xo (mm)**	**Dust Layer Height, Yd (mm)**
28	0.001867	0.000		
29	0.001933	0.036	15.5	
30	0.002000	0.103	44.0	
31	0.002067	0.170	72.6	
32	0.002133	0.236	100.7	
33	0.002200	0.303	129.2	1.8
34	0.002267	0.370	157.8	2.2
35	0.002333	0.436	185.9	2.9
36	0.002400	0.503	214.5	3.4
37	0.002467	0.570	243.0	3.4
38	0.002533	0.636	271.1	3.7
39	0.002600	0.703	299.7	3.9
40	0.002667	0.770	328.2	4.2
41	0.002733	0.836	356.3	4.6
42	0.002800	0.903	384.9	4.5
43	0.002867	0.970	413.4	4.8
44	0.002933	1.036	441.6	5.7
45	0.003000	1.103	470.1	5.1
46	0.003067	1.170	498.6	6.1
47	0.003133	1.236	526.8	6.6
48	0.003200	1.303	555.3	7.0
49	0.003267	1.370	583.9	7.1
50	0.003333	1.436	612.0	6.6
51	0.003400	1.503	640.5	7.0
52	0.003467	1.570	669.1	8.4
53	0.003533	1.636	697.2	9.1
54	0.003600	1.703	725.7	8.9
55	0.003667	1.770	754.3	9.0
56	0.003733	1.836	782.4	8.4
57	0.003800	1.903	810.9	8.1
58	0.003867	1.970	839.5	9.4
59	0.003933	2.036	867.6	9.7
60	0.004000	2.103	896.2	9.0
61	0.004067	2.170	924.7	9.3
62	0.004133	2.236	952.8	9.1

Table B4. Experimental data Run 2616, M = 1.35

Run 2616, M = 1.35				
Frame	**Capture Time (s)**	**Time after shock passage (ms)**	**Shock Front Propagation, Xs - Xo (mm)**	**Dust Layer Height, Yd (mm)**
25	0.001667	0.000		
26	0.001733	0.037	17.3	
27	0.001800	0.104	48.9	1.9
28	0.001867	0.171	80.5	2.4
29	0.001933	0.237	111.6	4.0
30	0.002000	0.304	143.1	4.4
31	0.002067	0.371	174.7	5.4
32	0.002133	0.437	205.8	5.5
33	0.002200	0.504	237.4	5.5
34	0.002267	0.571	269.0	6.3
35	0.002333	0.637	300.1	6.5
36	0.002400	0.704	331.7	8.0
37	0.002467	0.771	363.2	7.5
38	0.002533	0.837	394.3	8.9
39	0.002600	0.904	425.9	9.6
40	0.002667	0.971	457.5	10.4
41	0.002733	1.037	488.6	10.5
42	0.002800	1.104	520.2	12.7
43	0.002867	1.171	551.7	10.9
44	0.002933	1.237	582.9	10.9
45	0.003000	1.304	614.4	11.1
46	0.003067	1.371	646.0	13.3
47	0.003133	1.437	677.1	12.5
48	0.003200	1.504	708.7	11.3
49	0.003267	1.571	740.3	11.6
50	0.003333	1.637	771.4	11.6
51	0.003400	1.704	802.9	11.4
52	0.003467	1.771	834.5	12.0
53	0.003533	1.837	865.6	12.1
54	0.003600	1.904	897.2	13.4
55	0.003667	1.971	928.8	12.8
56	0.003733	2.037	959.9	11.4
57	0.003800	2.104	991.5	13.0
58	0.003867	2.171	1023.0	13.4
59	0.003933	2.237	1054.1	12.5

Table B5. Experimental data Run 2617, M = 1.38

Run 2617, M = 1.38				
Frame	**Capture Time (s)**	**Time after shock passage (ms)**	**Shock Front Propagation, Xs - Xo (mm)**	**Dust Layer Height, Yd (mm)**
25	0.001667	0.000		
26	0.001733	0.044	21.4	1.7
27	0.001800	0.111	53.7	1.8
28	0.001867	0.178	86.0	2.3
29	0.001933	0.244	117.8	3.0
30	0.002000	0.311	150.1	2.9
31	0.002067	0.378	182.5	4.3
32	0.002133	0.444	214.3	5.1
33	0.002200	0.511	246.6	5.2
34	0.002267	0.578	278.9	6.4
35	0.002333	0.644	310.8	6.6
36	0.002400	0.711	343.1	7.7
37	0.002467	0.778	375.4	7.8
38	0.002533	0.844	407.2	9.9
39	0.002600	0.911	439.5	9.1
40	0.002667	0.978	471.9	10.9
41	0.002733	1.044	503.7	11.3
42	0.002800	1.111	536.0	11.6
43	0.002867	1.178	568.3	11.0
44	0.002933	1.244	600.1	9.7
45	0.003000	1.311	632.5	10.0
46	0.003067	1.378	664.8	10.3
47	0.003133	1.444	696.6	10.5
48	0.003200	1.511	728.9	12.3
49	0.003267	1.578	761.2	12.5
50	0.003333	1.644	793.1	12.8
51	0.003400	1.711	825.4	11.6
52	0.003467	1.778	857.7	10.9
53	0.003533	1.844	889.5	11.6
54	0.003600	1.911	921.9	10.6
55	0.003667	1.978	954.2	10.4
56	0.003733	2.044	986.0	11.8
57	0.003800	2.111	1018.3	14.2
58	0.003867	2.178	1050.6	13.3
59	0.003933	2.244	1082.5	11.1

Table B6. Experimental data Run 2618, M = 1.39

Run 2618, M = 1.39				
Frame	**Capture Time (s)**	**Time after shock passage (ms)**	**Shock Front Propagation, Xs - Xo (mm)**	**Dust Layer Height, Yd (mm)**
24	0.001600	0.000		
25	0.001667	0.021	10.4	
26	0.001733	0.087	42.5	1.6
27	0.001800	0.154	75.1	1.8
28	0.001867	0.221	107.7	3.1
29	0.001933	0.287	139.9	4.2
30	0.002000	0.354	172.5	4.5
31	0.002067	0.421	205.1	4.7
32	0.002133	0.487	237.2	5.0
33	0.002200	0.554	269.8	5.9
34	0.002267	0.621	302.4	5.8
35	0.002333	0.687	334.6	6.9
36	0.002400	0.754	367.2	8.4
37	0.002467	0.821	399.8	9.1
38	0.002533	0.887	431.9	10.2
39	0.002600	0.954	464.6	10.4
40	0.002667	1.021	497.2	10.3
41	0.002733	1.087	529.3	9.0
42	0.002800	1.154	561.9	10.5
43	0.002867	1.221	594.5	9.7
44	0.002933	1.287	626.7	12.2
45	0.003000	1.354	659.3	13.2
46	0.003067	1.421	691.9	13.9
47	0.003133	1.487	724.0	11.6
48	0.003200	1.554	756.6	11.9
49	0.003267	1.621	789.2	10.0
50	0.003333	1.687	821.4	10.7
51	0.003400	1.754	854.0	11.0
52	0.003467	1.821	886.6	12.6
53	0.003533	1.887	918.7	12.1
54	0.003600	1.954	951.4	10.1
55	0.003667	2.021	984.0	12.1
56	0.003733	2.087	1016.1	12.1
57	0.003800	2.154	1048.7	12.0
58	0.003867	2.221	1081.3	13.9